A novel method to investigate tribological behaviors under transient temperatures using Pin-on-Cylinder tribometer and IR-thermography in glass forming

VU Anh Tuan[1,a] *, GRUNWALD Tim[2,b] and BERGS Thomas[1,c]

[1]Fraunhofer Institute for Production Technology IPT, Aachen, Germany

[2]Manufacturing Technology Institute (MTI), RWTH Aachen University, Aachen, Germany

[a]anh.tuan.vu@ipt.fraunhofer.de, [b]tim.grunwald@ipt.fraunhofer.de,
[c]thomas.bergs@ipt.fraunhofer.de

Abstract. In high-temperature material forming, achieving high precision demands a nuanced understanding of thermal and mechanical interactions at the contact interface. Conventional methods, often involving separate measurements of friction and heat transfer coefficients, encounter challenges as the growing number of influencing factors amplifies experimental complexity. This research introduces an innovative approach enabling the simultaneous determination of both coefficients in a single experimental run. A specially designed pin-on-cylinder tribometer enables the measurement of transient friction forces resulting from temperature variations at the interface, recorded by an infrared thermographic camera. Inverse methods are developed to derive the friction and heat transfer coefficients from the acquired transient force and temperature data. The method expedites the determination of contact coefficients, providing an efficient avenue for numerical and analytical studies in hot forming processes.

Introduction

Glass manufacturers are facing ever-growing demands from the optics market, necessitating advancements in manufacturing technologies to satisfy requirements consisting of increased geometrical complexity, high accuracy, energy-efficient production, and low-cost products. Nonisothermal Glass Molding (NGM) has emerged as a promising solution, enabling cost-efficient production of complex precision glass optics [1,2]. NGM involves the compression of a heated glass preform between two mold halves with lower temperatures, resulting in intricate heat exchanges and complex deformation behaviors at the glass-mold interface [3]. To achieve the required accuracy for precision optics, a comprehensive understanding of thermal-mechanical phenomena at glass-mold contact boundary, including friction and thermal conductance, is crucial.

In previous studies, the characterization of contact coefficients involved separate measurements of friction and contact heat transfer coefficients. While earlier works primarily explored the temperature-dependent nature of friction in glass forming [4], the influence of factors such as pressure, sliding velocity, and surface finish were investigated [5]. Similarly, contact heat transfer coefficients have been measured, considering temperature, pressure, and surface roughness [6]. However, conventional methods encounter challenges as the increasing number of influencing factors leads to a considerable rise in the number of experiments. Furthermore, numerous test setups have been developed to characterize friction and contact heat transfer individually, contributing to the complexity of the experimental process. For example, ring compression [7], double shear test [8], and pin-on-disc [9] have been reported for the friction measurement. For the contact heat transfer measurement, both steady-state [10] and transient methods [11] have been explored. The latter method demonstrated a highly time-efficient approach for determining contact heat transfer coefficients, varying with temperature, pressure, and surface roughness.

This research addresses the limitations of conventional methods by introducing a novel approach using a Pin-on-Cylinder (PoC) tribometer. The tribometer, equipped with an infrared thermography camera (IR-camera), allows for the simultaneous measurement of transient temperatures of contacting materials near the contact point. By solving the inverse heat transfer problem, contact heat transfer coefficients can be derived from transient temperature measurements. Concurrently, the variation of transient friction force with temperature can be recorded, enabling the derivation of friction coefficients. The experimental setup and the application of inverse heat transfer solutions to determine friction and contact heat transfer coefficients are elaborated in the subsequent chapter. This innovative method offers a more efficient and integrated approach to characterizing contact coefficients in glass forming processes.

Experimental setup

To achieve the research goal, this study constructed a novel tribometer based on the pin-on-cylinder principle. The tribometer incorporates the analogy method proposed for studying friction by Zemzemi et al. [12] and the inverse method for exploring transient contact heat transfer in glass forming using the IR-camera introduced by Vu et al. [13]. The new tribometer aims to investigate the process parameters as key factors influencing friction and heat transfer between glass and steel materials at elevated temperatures, emphasizing nonisothermal conditions where the temperatures of the glass and steel differ. This deliberate non-uniformity mimics realistic scenarios encountered in various glass forming processes, enhancing the study's practical relevance.

Fig. 1 introduces the tribometer setup and its key components. The apparatus, affixed to a lathe slide, featured a centered and securely clamped steel cylinder. To prevent the cylinder bending during operation, two rollers as a counter holder provided firm support. In the friction experiment, the cylinder was rotated (ω), while the glass pin was constantly pressed onto the cylinder with a normal force (F_N) by a hydraulic unit and traversed linearly (v) along the cylinder. This dynamic combination of axial feed and rotational speed enabled the continual creation of new contact points as the pin traversed the cylinder. This process aimed to level surface roughness and induced material hardening through multiple traversals along the friction path. Moreover, the resulting helical trajectory of the pin on the cylinder allowed for the deformation of previously unaffected material, even after a full rotation of the cylinder.
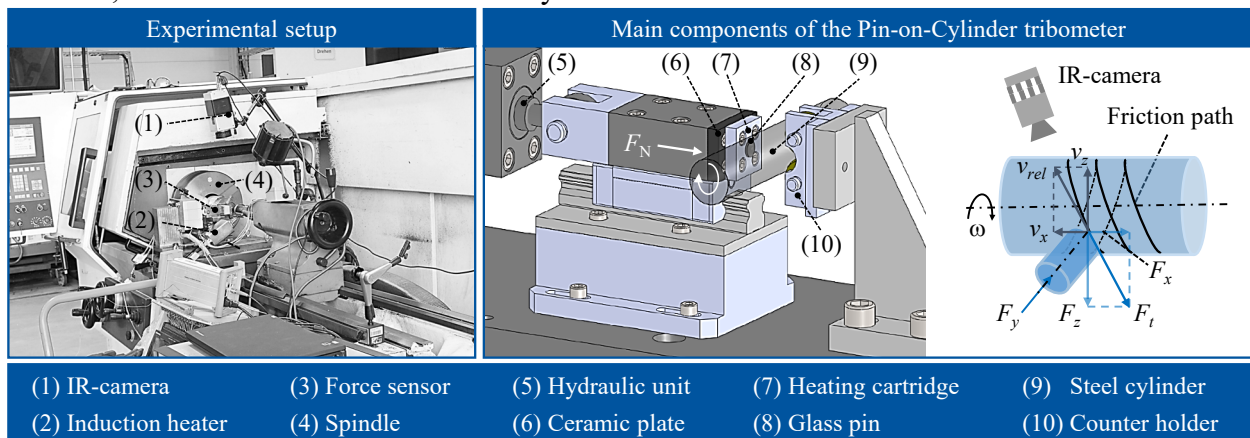

Experimental setup		Main components of the Pin-on-Cylinder tribometer		
(1) IR-camera	(3) Force sensor	(5) Hydraulic unit	(7) Heating cartridge	(9) Steel cylinder
(2) Induction heater	(4) Spindle	(6) Ceramic plate	(8) Glass pin	(10) Counter holder

Fig. 1. Experimental setup and components of the PoC tribometer.

Heating methods. Two distinct methods were employed for heating the specimens. The steel cylinder underwent induction heating by being placed within two copper rings, while the glass pin, held in a clamping holder, was heated using a heating cartridge. Additionally, to protect the force sensor, positioned directly behind the glass specimen, from thermal interference, a ceramic insulation was placed between the heating cartridge and the force sensor. This setup enabled the glass pin to be heated to temperatures exceeding the glass transition temperature T_g ($T_g = 557\ °C$).

Measuring data acquisition. For precise measurement in the tribological tests, accurate data necessitates capturing process forces and temperature variations at the contact interface. Process forces were recorded using a three-component force measurement platform, capable of determining dynamic and static forces in three orthogonal directions (F_x, F_y, and F_z) as depicted in Fig. 1. This platform utilized piezo elements with force-proportional charge displacements, and the signals were processed by a charge amplifier and LabVIEW software. Variable amplification and filtering were applied, including a low-pass filter with a 1 kHz cut-off frequency. Simultaneously, transient temperatures of the glass and cylinder were monitored using an infrared thermographic camera (VarioCAM®HD head, InfraTec). The camera, with a temperature measuring range up to 2000°C and an accuracy of ±1°C, captured thermal radiation in the spectral range from 7.5 to 14 µm at a full-frame rate of 30 Hz. For the ease of imaging data analysis and accurate measurement data using IR thermographic techniques, both glass and cylinder surfaces were coated with high-temperature resistant black layers, possessing an emissivity of approximately 0.9. These thin black layers not only enhance measurement accuracy by minimizing the influence of surrounding radiation reflected at the measuring surfaces but also precisely determine the emissivity of both specimens across broad temperatures set for the IR-camera [13].

Samples' preparation. Contrasting with the PoC setup utilized in the prior work by Hild et al. [14], the tribometer employed in this present study involved an adaptation to essentially enable high-temperature tribological tests for glass-forming experiments. During these tests, deformation primarily occurred in the glass, making temperature homogeneity crucial for understanding the material behaviors of glass, specifically thermoviscoelastic deformation [15,16], and for subsequent inverse analysis. Hence, the pin was crafted from N-BK7 glass, a commonly used composition in glass molding processes, and a high-temperature-resistant steel grade, 1.4181 (AISI 314), was employed for the cylinder, given its widespread use as a mold material in NGM processes [17,18]. The thermal and mechanical properties of the materials used for the samples are given in Table 1. It is emphasized that prior to tribo-experiments, a sufficiently long heating period was carefully identified aiming to homogenize the temperatures of the specimens.

Table 1. Thermal- and mechanical properties of glass pin and steel cylinder

Thermal properties	Unit	N-BK 7	1.4181 steel
Density, ρ	kg/m^3	2510	7900
Thermal conductivity, λ	W/mK	1.114	15
Specific heat, C_p	J/kgK	858	500
Young modulus, E	GPa	82	196
Poisson's ratio, ν	1	0.206	0.28
Glass transition temperature, T_g	°C	557	-

Although it is commonly agreed that surface roughness is a factor influencing on the thermal and mechanical phenomena at the contact interface, the present study does not explicitly consider its impact. Special attention was devoted to surface preparation, with the objective of ensuring identical surface roughness for all test samples. The glass specimens underwent fine grinding and polishing procedures following the specifications outlined in DIN ISO 10110, achieving the surface finish equivalent to P3 grade with Ra = 8-16 nm. The cylindrical samples were precision-machined through turning, followed by a subsequent polishing process achieving surface roughness varying in the range Ra = 40-80 nm (P2 grade).

Methodology
Building upon the newly developed PoC tribometer setup, this study introduces methods that enable the concurrent determination of contact heat transfer and friction coefficients in a single operation, through either *sequential approach* or *parallel approach*.
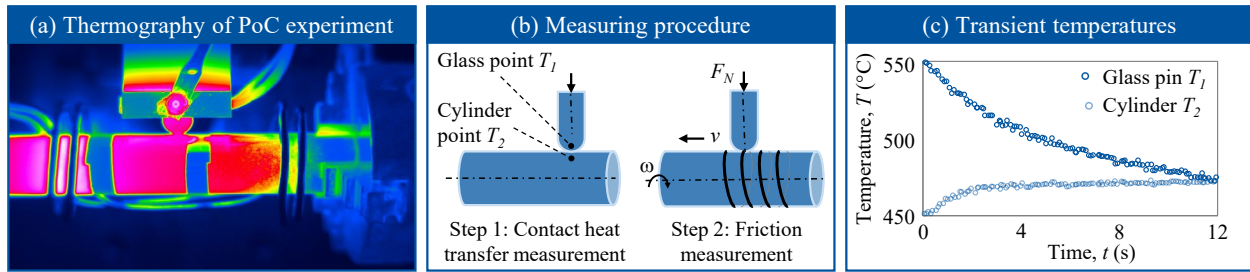
Fig. 2. (a) Thermographic image of a PoC experiment, (b) procedure of the sequential method and measuring points by the IR-camera, and (c) transient temperatures of the specimens during the contact heat transfer measurement.

Sequential approach. This approach was designed to measure the contact heat transfer coefficient before conducting friction measurements in a quasi-isothermal process. Specifically, the glass and cylinder specimens were individually heated using the heating cartridge and induction, respectively, reaching predefined temperatures. Subsequently, the glass was brought into contact with the cylinder at a specified normal force, with no sliding velocity applied during the contact heat transfer measurement. Fig. 2a introduces a thermographic image of the specimens. Throughout the contact heat transfer measurement period, the IR-camera (see Fig. 2b) captured transient temperatures near the contact point, which were then utilized to calculate the contact heat transfer coefficient. The friction measurement began when the temperatures of the specimens were nearly identical. In this phase, a constant rotational speed of the cylinder and pin feed were applied, and process forces were collected under a constant normal force to derive the friction coefficients.

Parallel approach. This approach focused on measuring friction coefficients under a nonisothermal process, utilizing heat transfer at the glass-cylinder interface and variations in glass temperature at the contact point to derive the contact heat transfer coefficient. After heating, the specimens were brought into contact, initiating measurements of process forces and glass temperature. Throughout the measurement, the normal force and rotational speed are held constant.

Inverse heat transfer solutions. The contact heat transfer coefficient, quantifying the heat flow through the interface, hinges on the knowledge of two variables: the heat flux ($\dot{q}''$) and the temperature difference (ΔT) as defined by Eq. 1. The latter is determined by the temperatures of the contacting materials–the glass specimen (T_1) and the cylinder (T_2). While the IR-camera allows measurement of transient temperatures, the heat flux remains unknown. For this reason, the coefficient cannot be directly measured through the thermographic method. Consequently, the derivation of the contact heat transfer coefficient necessitates inverse heat transfer solutions [19].

$$h_c = \frac{\dot{q}''}{\Delta T} = \frac{\dot{q}''}{T_1 - T_2}. \tag{1}$$

In sequential method, the contact point remains fixed throughout the contact heat transfer measurement. As a result, it permits the IR-camera to consistently capture the same measuring points of the glass and the cylinder near the contact interface during the measuring period. Fig. 2c shows a plot of transient temperature profiles of the measuring points during the recording period t, $T_{i,exp}(t)$ ($i = 1,2$). The objective of the inverse solution is to iteratively estimate the heat flux until achieving a precise calculation of the transient temperatures of the contacting materials. In each iteration, the temperature of each specimen is computed using the energy balance equation:

$$\rho \cdot C_p \cdot \frac{\partial T}{\partial t} = \lambda \cdot \frac{\partial^2 T}{\partial x^2} - h_{eff} \cdot \frac{P}{A} \cdot (T - T_\infty), \text{ with } \dot{q}'' = -\lambda \frac{\partial T}{\partial x}. \tag{2}$$

where ρ, C_p and λ are the thermal properties of the specimens given in Table 1; h_{eff} denotes the effective heat transfer coefficient, comprising of both convective and radiative heat losses to the environment at a specific ambient temperature T_∞; P and A are the perimeter and area, respectively; and x is the position where the node temperature is calculated.

Eq. (2) provides the computed temperatures throughout the measuring period of the specimens, referred as $T_{i,est}(t)$. If the disparity between the measured and computed temperatures exceeds an acceptable tolerance, the computed temperature requires correction by estimating a new heat flux through the conjugate gradient method [20]. This iterative procedure aims to refine the transient heat flux $\dot{q}''(t)$ by minimizing an objective function $\Omega\left(\dot{q}''(t)\right)$, defined as:

$$\Omega\left(\dot{q}''(t)\right) = \int_0^t \left(T_{i,exp}(\xi) - T_{i,est}(\xi)\right)^2 d\xi \rightarrow \min. \tag{3}$$

In Eq. (3), $T_{i,exp}(\xi)$ and $T_{i,est}(\xi)$ are the vectors containing the measured and estimated temperatures, respectively, taken at a given time ξ ($0 < \xi < t$). Fig. 3a illustrates the flowchart of the inverse procedure employed in the sequential method. Details of the iterative procedure for solving inverse heat transfer problem using the conjugate gradient method can be found in [13].
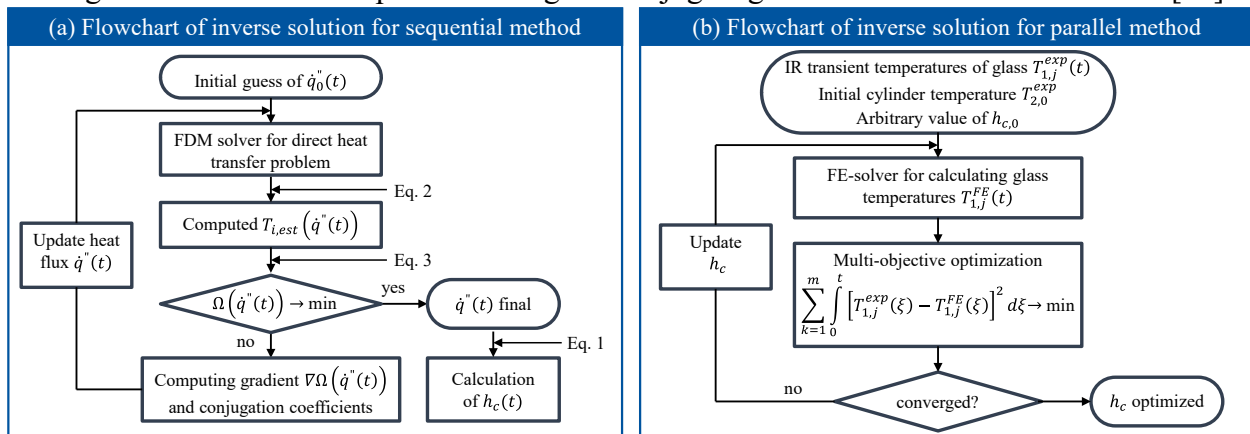

Fig. 3. Flowcharts of inverse solutions for determining the contact heat transfer coefficients.

In parallel approach, deriving the contact heat transfer coefficient from the direct temperature measurement of the contact pair proves more demanding. This difficulty arises because the cylinder rotates continuously during the measuring period of the contact heat transfer and friction coefficients. Because of the rotation, the glass pin consistently encounters new contact points on the cylinder, forming a helical friction path as schematically depicted in Fig. 1. Since the IR-camera was configured to measure temperatures at the contact points, the temperature of the glass pin can be recorded from a fixed point. However, the temperature reading of the cylinder follows the friction path, resulting in signal oscillations. Consequently, the oscillating measured data can pose an ill-posed problem when solving the inverse heat transfer using the conjugate gradient method [20], as approached in the sequential method.

To address this challenge, an FE-inverse approach was proposed. Specifically, a numerical model of the PoC setup was established to solve the nonlinear heat exchanges at the contact interface. The inputs for this model included the transient temperature measurements of the glass specimen $T_1(t)$ and the constant and homogeneous initial temperature of the cylinder $T_2(t = 0)$. Initially, an arbitrary contact heat transfer coefficient was given, which then allows for the estimation of temperatures at corresponding points on the glass as captured by the IR-camera. The estimated temperatures were then compared with those measured experimentally. Subsequent iterative simulations were carried out through a fully automated routine scripted in Python, aiming

to minimize the differences between the transient temperatures by updating new contact heat transfer coefficients. The flowchart of this procedure is described in Fig. 3b.

Finally, the derivation the friction coefficient using the PoC tribometer necessitates a particular procedure. As depicted in Fig. 1, the force sensors included the three components of the process force signals, from which the normal force and tangential force were computed. However, the measured tangential force encompassed not only the friction force but also the force required to deform the specimens. To calculate the actual friction coefficient, an iterative approach utilizing FEM simulations of the tribometer, as elucidated in [12], was performed. Initially, friction was modeled with the apparent friction coefficient calculated from experimentally measured process forces. The difference between the tangential force extracted from the simulation and the experimental data was assumed to be the force resulting from the samples' deformation. A new friction coefficient was then calculated from the experimental data, and this process repeated until the difference between the apparent friction coefficient from the simulation and the experimental value can be negligible. Leveraging the PoC apparatus and this computational approach, variations in the normal force, rotational speed, and specimen temperature allowed for the investigation of friction coefficients based on contact normal stress, relative velocity, and interfacial temperature.

Results

The contact heat transfer coefficients determined through the sequential approach are shown in Fig. 4. In Fig. 4a, the transient contact heat transfer coefficient $h_c(t)$ is computed based on the measured transient temperatures of the two specimens. The plot presents the result of a contact pair where the initial temperatures of glass and cylinder are 550 °C and 500 °C (550/500 °C), respectively, under the applied pressure of 24 MPa. The transient coefficient exhibits a significant increase as soon as the glass pin contacted the cylinder, followed by a steady-state process. It is noteworthy that the initial surge in the coefficient aligns with the rise in contact pressure [11]. Once the predefined contact pressure was attained, the variation in the contact heat transfer coefficient became slight and stabilized after 4 seconds. Therefore, the plot exhibits the temperature variations of the contact pair within a 4-second period, and the coefficient was considered steady-state after this duration.
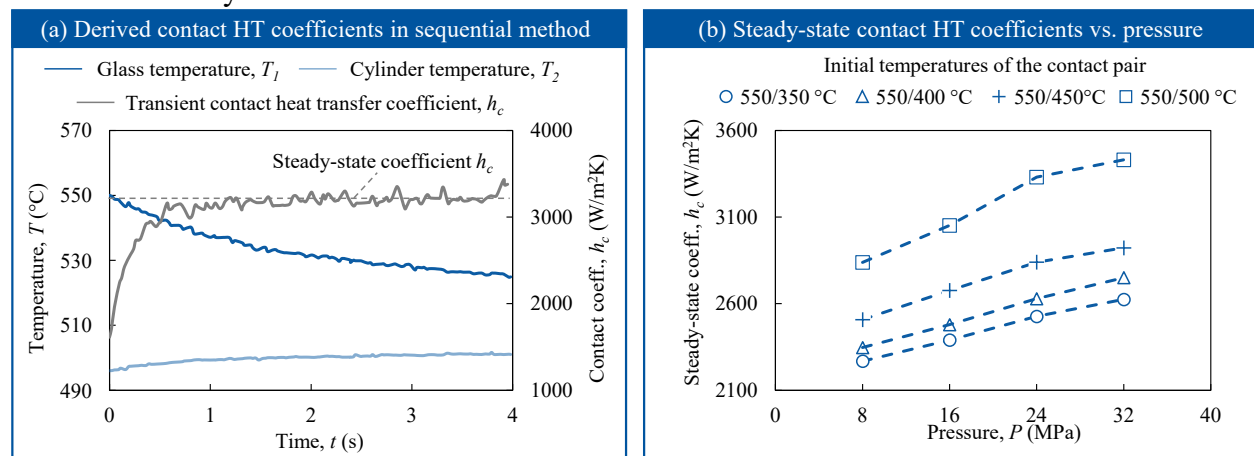

Fig. 4. (a) Derivation of contact heat transfer coefficient from the measured temperatures in the sequential method, and (b) dependence of contact coefficients on pressure and initial temperatures of the contact pair.

Furthermore, the influences of the contact pressure and the temperatures of the contact pair were examined, and the results are presented Fig. 4b. For these investigations, a glass temperature of 550 °C, close to the glass transition temperature T_g, was chosen for all experiments, while the cylinder temperatures were varied within the range of 350 °C to 500 °C. The results clearly demonstrate a strong dependency of the pair temperature on the contact heat transfer coefficients.

When the glass pin was brought into contact with a higher cylinder temperature, it led to a higher interfacial temperature. Consequently, the elevated interfacial temperature promoted deformation of the contact pair, resulting in an increased contact area. With the enlargement of the contact area, more heat transfer occurs through the contact. Moreover, the contact pressure additionally contributes to the growth of the contact area; hence, higher applied contact pressures increase the contact heat transfer coefficients. It is observed that the contact heat transfer coefficients linearly increase with the applied pressures at low interfacial temperatures. However, when the interfacial temperature is sufficiently high, such as 550/500 °C, where the interfacial temperature is close to the glass transient temperature T_g, the growth of contact heat transfer coefficients become nonlinear. The linear increase of the contact heat transfer coefficients in the low interfacial temperature range is attributed to the elastic behavior of the material pair, where the deformations of the pair linearly increase with the applied pressures. However, at a temperature in the glass transition region, the glass deformation is dominated by a viscoelastic response, which is thermal-history-, pressure-, and time-dependent [21]. Ultimately, the combined elastic-viscoelastic deformation behaviors of the material pair contribute to the nonlinear increase of the contact heat transfer coefficients concerning pressure and interfacial temperature.

In Fig. 4b, the pressures are referred to the locally normal contact stresses at the pin-cylinder contact point. The contact stresses were derived from the applied forces using the Hertzian theory of contact for sphere-cylinder elastic solids [22]. The material properties necessary for calculating the contact stress were obtained at room temperature, given in Table 1. In the present study, we assumed a constant contact pressure throughout the measuring period, corresponding to the initial applied force. This assumption implies that the contact area, influenced by the macroscopic deformation of glass, remained unchanged. The implications of any contact pressure variation resulting from the macroscopic deformation, governed by the stress relaxation phenomenon of glass, will be thoroughly discussed in the forthcoming paper.
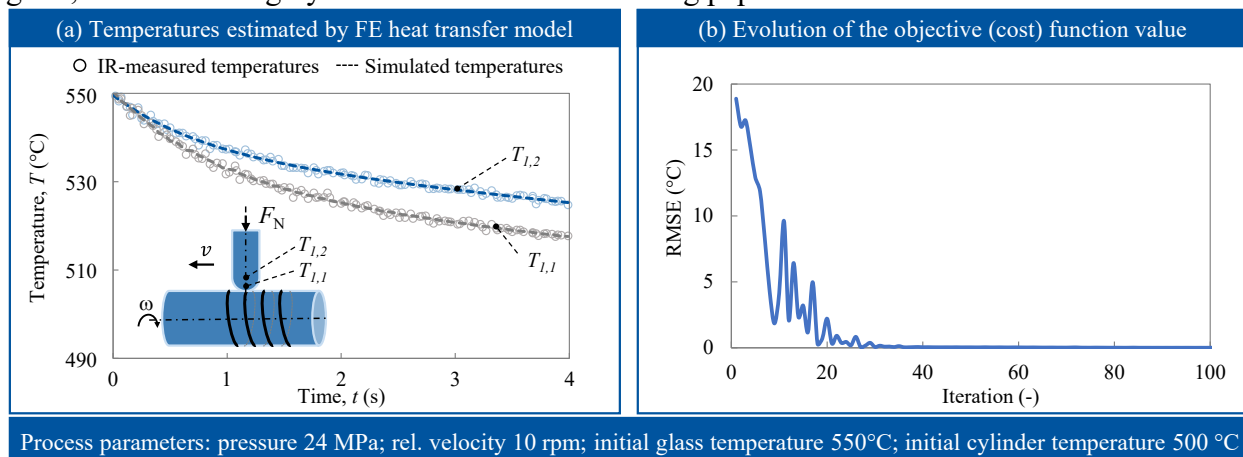

Fig. 5. Determination of contact heat transfer coefficient from the measured temperatures in the parallel method.

Fig. 5 presents the results of inverse computation of the contact heat transfer coefficients in the parallel method. In Fig. 5a, the transient temperature profiles of two points (sensors) measured on the surface of the glass pin are plotted. The first point $T_{1,1}$ was extracted directly adjacent to the contact interface, and the other $T_{1,2}$ was positioned 1 mm further from the interface. As described in Fig. 3b, an FE model was built and served as the nonlinear numerical solver for the inverse contact heat transfer simulation. The iterative estimation of transient temperatures for the identified sensors involved varying the contact heat transfer coefficient.

The results demonstrate a noteworthy agreement between the estimated temperatures obtained through the FE model and experimental measurements, emphasizing the efficacy of the multi-

objective solution. The convergence plot in Fig. 5b shows that approximately 40 iterations suffice to optimize the contact heat transfer coefficient, emphasizing the efficiency of the proposed approach. The derived contact heat transfer coefficient for this example in the parallel method was found comparable to that obtained through the sequential approach.

Finally, Fig. 6 presents the process forces obtained during the friction measurement (Fig. 6a) and the resultant Coulomb friction coefficients derived from these measured forces across various contact temperature experiments (Fig. 6b). The Coulomb's friction law was considered, a choice supported by its extensive application in prior research, underscoring its efficacy in predicting the macroscopic deformation of glass and the form accuracy of molded glass optics. This relevance persists even under high contact pressures typical in glass forming processes [7,10]. The friction coefficients, shown in Fig. 6b, are calculated upon reaching the predefined normal force, with error bars indicating the oscillation inherent in the recorded forces throughout the friction measurement.
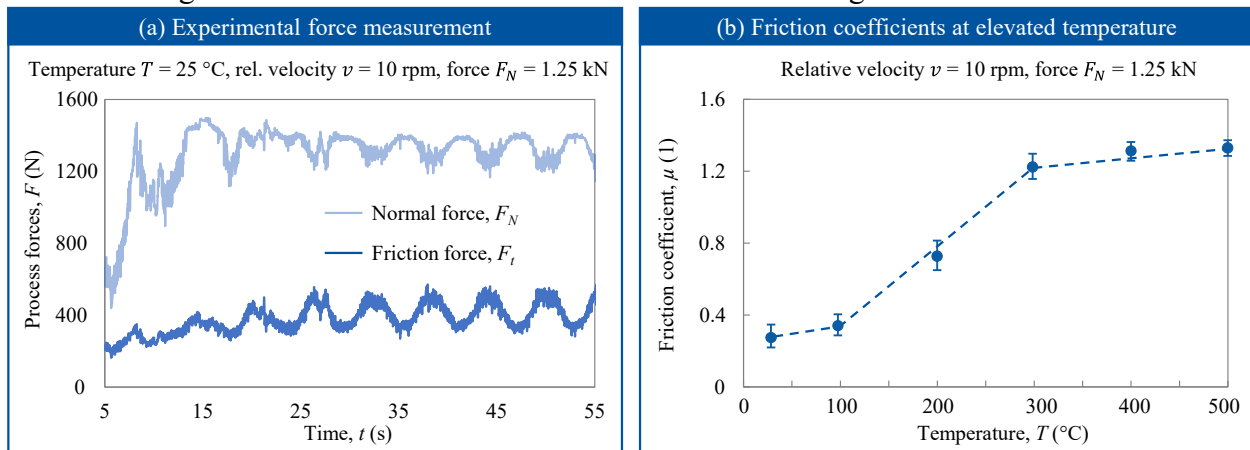

Fig. 6. (a) Process forces during the friction measurement, and (b) friction coefficient vs. temperature.

The results illustrate a noticeable escalation in the friction coefficient with increasing contact temperature, consistent with observations in previous works [5]. However, our findings reveal a more pronounced change in the friction coefficient at temperatures well below the glass transition temperature T_g, while the effect becomes less significant at temperatures near T_g. At low temperature range near room temperature, glass exhibits significant elasticity, leading to hard contact at the interface. Ploughing, arising from the sliding of two solid surfaces at both macroscopic and microscopic levels, contributes as the primary mechanism, resulting in a monotonic increase in friction forces. The more noticeable increase of friction coefficients in the following temperature range is explained by the surface fracturing of the glass specimens. In this range, glass is not in the glass transition, inherently exhibiting brittleness without significant deformation before fracturing occurs. In contrast, as temperature rises further, approaching the glass transition region (near T_g), the variation in friction becomes less significant. This can be elucidated by the fact that the increase in friction caused by fracturing is mitigated by the substantial reduction in the modulus and hardness of the steel pin. Moreover, the primary influence on friction in this temperature range is the relaxation phenomenon inherited by the viscoelastic deformation of glass. Due to the stress relaxation, the flow stress tends to decrease after small straining when it is approaching the glass transition region.

The current study aims to present a method that facilitates the simultaneous determination of contact heat transfer and friction coefficients within the PoC tribometer. The findings, depicted in Fig. 6, highlights the influences of temperature on frictional behavior near the glass transition temperature, demonstrating consistent findings with prior investigations using alternative methods

like the pin-on-disc tribometer [23]. In further study, comprehensive insights into temperature- and pressure-dependent friction coefficients within the glass transition region will be discussed.

Summary

This study addresses the essential understanding of thermal-mechanical interactions at contact interfaces, a crucial aspect in controlling material forming processes. A novel characterization method is introduced, enabling the simultaneous determination of contact heat transfer and friction coefficients using a single tribometer and a singular operational run. Two distinct approaches are presented, each necessitating a specific inverse method. Utilizing the proposed tribometer setup and methodology, critical factors influencing contact coefficients can be explored. The versatility of this setup extends its applicability to diverse material forming processes, providing an efficient means to comprehend these processes and enhance product quality control.

Acknowledgement

References

[1] H. Kreilkamp, A.T. Vu, O. Dambon, F. Klocke, Replicative manufacturing of complex lighting optics by non-isothermal glass molding, in: D.H. Krevor (Eds.), Polymer Optics and Molded Glass Optics: Design, Fabrication, and Materials 2016, SPIE, 2016, 99490B. https://doi.org/10.1117/12.2235848

[2] H. Kreilkamp, A.T. Vu, O. Dambon, N.F. Klocke, Non-Isothermal Glass Molding of Complex Led Optics, in: S.K. Sundaram (Ed.), 77th Conf. on Glass Problems, Wiley, 2017, pp. 141–149. https://doi.org/10.1002/9781119417507.ch13

[3] A.T. Vu, G. Liu, H. Kreilkamp, O. Dambon, F. Klocke, Numerical modeling-based design of the newly developed nonisothermal glass molding process for complex glass optics, in: Glass Service (Ed.), 13th International Seminar on Furnace Design – Operation & Process Simulation, Czech Republic, 2015, p.376–390.

[4] B. Ananthasayanam, D. Joshi, M. Stairiker, M. Tardiff, K.C. Richardson, P.F. Joseph, High temperature friction characterization for viscoelastic glass contacting a mold, Journal of Non-Crystalline Solids 385 (2014) 100–110. https://doi.org/10.1016/j.jnoncrysol.2013.11.007

[5] P. Mosaddegh, S. Akbarzadeh, M. Zareei, H. Reiszadeh, Tribological behavior of BK7 optical glass at elevated temperatures, Proceedings of the Institution of Mechanical Engineers, Part J: Journal of Engineering Tribology 233 (2019) 580–592. https://doi.org/10.1177/1350650118788756

[6] A.T. Vu, S. Gulati, P.-A. Vogel, T. Grunwald, T. Bergs, Machine learning-based predictive modeling of contact heat transfer, Int. Journal of Heat and Mass Transfer 174 (2021) 121300. https://doi.org/10.1016/j.ijheatmasstransfer.2021.121300

[7] A. Sarhadi, J.H. Hattel, H.N. Hansen, Evaluation of the viscoelastic behaviour and glass/mould interface friction coefficient in the wafer based precision glass moulding, Journal of Materials Processing Technology 214 (2014) 1427–1435. https://doi.org/10.1016/j.jmatprotec.2014.02.008

[8] P. Mosaddegh, J.C. Ziegert, Friction measurement in precision glass molding: An experimental study, Journal of Non-Crystalline Solids 357 (2011) 3221–3225. https://doi.org/10.1016/j.jnoncrysol.2011.05.012

[9] J. Zhou, H. Xu, C. Zhu, W. Ai, X. Liu, K. Liu, High-temperature friction characteristics of N-BK7 glass and their correlation with viscoelastic loss modulus, Ceramics International 47 (2021) 21414–21424. https://doi.org/10.1016/j.ceramint.2021.04.151

[10] T.D. Pallicity, A.T. Vu, K. Ramesh, P. Mahajan, G. Liu, O. Dambon, Birefringence measurement for validation of simulation of precision glass molding process, J Am Ceram Soc 100 (2017) 4680–4698. https://doi.org/10.1111/jace.15010

[11] A.T. Vu, T. Helmig, A.N. Vu, Y. Frekers, T. Grunwald, R. Kneer, T. Bergs, Numerical and experimental determinations of contact heat transfer coefficients in nonisothermal glass molding, J Am Ceram Soc 103 (2020) 1258–1269. https://doi.org/10.1111/jace.16756

[12] F. Zemzemi, J. Rech, W. Ben Salem, A. Dogui, P. Kapsa, Identification of a friction model at tool/chip/workpiece interfaces in dry machining of AISI4142 treated steels, Journal of Materials Processing Technology 209 (2009) 3978–3990. https://doi.org/10.1016/j.jmatprotec.2008.09.019

[13] A.T. Vu, A.N. Vu, G. Liu, T. Grunwald, O. Dambon, F. Klocke, T. Bergs, Experimental investigation of contact heat transfer coefficients in nonisothermal glass molding by infrared thermography, J Am Ceram Soc 102 (2019) 2116–2134. https://doi.org/10.1111/jace.16029

[14] R. Hild, D. Trauth, P. Mattfeld, S. Bastürk, T. Brögelmann, N. Kruppe, K. Bobzin et al., Trockenumformung strukturierter Halbzeuge aus 16MnCr5 und 42CrMo4*/Dry forming of surface structured workpiece made of 16MnCr5 and 42CrMo4 - Determination of friction shear stress by means of a pin-on-cylinder Tribometer, wt 106 (2016) 712–718. https://doi.org/10.37544/1436-4980-2016-10-38

[15] A.T. Vu, A.N. Vu, T. Grunwald, T. Bergs, Modeling of thermo-viscoelastic material behavior of glass over a wide temperature range in glass compression molding, J Am Ceram Soc 103 (2020) 2791–2807. https://doi.org/10.1111/jace.16963

[16] A.T. Vu, T. Grunwald, T. Bergs, Thermo-viscoelastic Modeling of Nonequilibrium Material Behavior of Glass in Nonisothermal Glass Molding, Proc. Manufacturing 47 (2020) 1561–1568. https://doi.org/10.1016/j.promfg.2020.04.350

[17] A.T. Vu, H. Kreilkamp, O. Dambon, F. Klocke, Nonisothermal glass molding for the cost-efficient production of precision freeform optics, Opt. Eng 55 (2016) 71207. https://doi.org/10.1117/1.OE.55.7.071207

[18] A.T. Vu, P.A. Vogel, A. Siva Subramanian, T. Grunwald, T. Bergs, Real-Time Quality Control in Thin Glass Forming Using Infrared Thermography and Deep Learning, KEM 926 (2022) 2312–2321. https://doi.org/10.4028/p-5w9vr9

[19] C. Fieberg, R. Kneer, Determination of thermal contact resistance from transient temperature measurements, International Journal of Heat and Mass Transfer 51 (2008) 1017–1023. https://doi.org/10.1016/j.ijheatmasstransfer.2007.05.004

[20] M.N. Ozisik, H. Orlande, A.J. Kassab, Inverse Heat Transfer: Fundamentals and Applications, Applied Mechanics Reviews 55 (2002) B18-B19. https://doi.org/10.1115/1.1445337

[21] A.T. Vu, R.d.l.A. Avila Hernandez, T. Grunwald, T. Bergs, Modeling nonequilibrium thermoviscoelastic material behaviors of glass in nonisothermal glass molding, J Am Ceram Soc 105 (2022) 6799–6815. https://doi.org/10.1111/jace.18605

[22] V.L. Popov, Contact Mechanics and Friction, Springer Berlin Heidelberg, Berlin, Heidelberg, 2010.

[23] P. Chizhik, M. Friedrichs, D. Dietzel, A. Schirmeisen, Tribological Analysis of Contacts Between Glass and Tungsten Carbide Near the Glass Transition Temperature, Tribol Lett 68 (2020). https://doi.org/10.1007/s11249-020-01363-0